Stable Blue Luminescent CsPbBr 3 Perovskite Nanocrystals Confined in Mesoporous Thin Films

Victor Malgras, Joel Henzie, Toshiaki Takei, Yusuke Yamauchi

Stable Blue Luminescent $CsPbBr_3$ Perovskite Nanocrystals Confined in Mesoporous Thin Films

Victor Malgras[a], Joel Henzie[b]*, Toshiaki Takei[b], and Yusuke Yamauchi[c,d,e]*

Abstract: Creating $CsPbBr_3$ perovskite nanocrystals with bright blue emission is challenging because their optical properties depend sensitively on structure, which can be influenced by colloidal purification procedures. Growing perovskites in mesoporous templates bypasses some of these purification issues because the size of the nanocrystal is governed by the dimensions of the pores. Mesoporous silica consisting of aligned channels with tunable diameter can be easily synthesized and used as template. In SBA-15 films the mesoporous channels are interconnected by numerous ~1.5 to 4.0 nm diameter (*d*) smaller pores. These openings help fill the templates with perovskite precursor solution because they prevent dead-end channels. When the perovskite solution evaporates and retreats, some of the liquid remains trapped in the interconnecting pores by discontinuous dewetting. The precursor crystallizes, generating stable *d* ~ 3.1 nm blue-emitting perovskite nanocrystals. The mesoporous template also serves as a protective barrier to preserve the optical properties of the $CsPbBr_3$ from atmospheric conditions. Besides the significant blue-shift of the luminescence peak, we observed a decrease of the longer lifetime component in the film, accompanied by a strong increase of the external quantum efficiency.

The optoelectronic properties of bulk lead halide perovskites have enabled a whole new class of inexpensive, efficient, solution processable light-emitting and light-harvesting devices. Doping and alloying approaches have long served as an effective means of tuning the optical properties of semiconductors. But nanostructuring is a parallel and complementary strategy to control the excitonic band gap, as well as relaxation, recombination and energy transfer dynamics.[1] Colloidal lead halide perovskite nanocrystals (NCs) have been generated using various routes including hot injection synthesis,[2] room temperature crystallization,[3] and various microemulsion methods.[4] Methylammonium lead bromide ($MAPbBr_3$) perovskites NCs are known for their bright green emission, possessing photoluminescence quantum yields (PLQY) close to unity.[5] Cesium lead bromide ($CsPbBr_3$) NCs are an all-inorganic perovskite counterpart that are more stable than $MAPbBr_3$, and have already achieved PLQY values > 90%.[2] To our knowledge, there are few reports of blue-emitting cesium-based perovskite NCs because band gaps in the blue region require the nanoparticle to have one dimension < 4 nm. This is challenging due to material stability issues, and to the polydisperse nature of most synthetic colloidal methods.[6] Ultrathin two-dimensional (2D) $CsPbBr_3$ nanoplates exhibit blue emission, although their ionic nature makes them susceptible to degradation.[7] Integrating these kinds of colloids into devices is a challenging task, because their sensitivity to water will require all the synthesis, purification and fabrication to be carried out in an inert atmosphere.

To realize a simple and reliable bench-top method to generate stable blue-emitting all-inorganic perovskite nanoparticles, we used ordered mesoporous silica films as templates to direct and confine the growth of nanocrystals. Nanoporous matrices offer numerous advantages in the synthesis of nanostructured lead halide perovskite materials in particular.[8] Mesoporous templates provide a ligand-free approach to prevent aggregation, and depending on the dielectric properties of the template it can interconnect or isolate the NCs electronically and optically. For example, silica is ideal for studying the properties of isolated nanoparticles, because its insulating nature contributes minimal collateral electronic interactions. In addition, the natural encapsulation limits adventitious exposure to water, promoting NC stability. Compared to their powdered counterparts, mesoporous thin films yield larger periodic domains (> 1 µm) with a fixed orientation relative to the substrate. Well-ordered structures can even lead to monodisperse particles arranged according to the negative replica of the mold. We envisioned film templates as a platform towards functional composites that are "ready-for-integration", whereas mesoporous powders require further processing steps that cause additional challenges. Finally, films produce negligible scattering in the active region of the device since, unlike the typical micrometer grain size in powders, their features are far below the diffraction limit of light (<< λ).

Capillarity is the main driving force for infusing the channels of the template with perovskite precursor solution. As the diameter (*d*) of the channel decreases below some threshold, nanofluidic effects begin impacting viscosity and restraining mass transport, thus limiting effective filling of the template.[9] In order to circumvent this nanofluidic hindrance, we sought to exploit a well-known property the mesoporous SBA-15 family: its hierarchical porous composition. The main mesochannels are the negative replica of the cylindrical micelles arranged in a 2D hexagonal phase and separated by the aqueous domain where the hydrolitic condensation of SiO_2 occurs. Two additional categories of micropores are also present:[10] i) ultramicropores (< 1 nm): small pockets that are the imprint of the hydrophobic polyethylene oxide (PEO) subunits on the surface of the

[a] Dr. V. Malgras
International Center for Young Scientists (ICYS)
National Institute for Materials Science (NIMS)
1-1 Namiki, Tsukuba, Ibaraki 305-0044 (Japan)

[b] Dr. J. Henzie, Dr. T. Takei
International Centre for Materials Nanoarchitectonics (MANA)
National Institute for Materials Science (NIMS)
1-1 Namiki, Tsukuba, Ibaraki 305-0044, Japan
E-mail: Henzie.Joeladam@nims.go.jp

[c] Prof. Y. Yamauchi
College of Chemistry and Molecular Engineering
Qingdao University of Science and Technology
Qingdao 266042, China

[d] Prof. Y. Yamauchi
Department of Plant & Environmental New Resources
Kyung Hee University, 1732 Deogyeong-daero, Giheunggu,
Yongin-si, Gyeonggi-do 446-701, South Korea

[e] Prof. Yamauchi
School of Chemical Engineering & Australian Institute for Bioengineering and Nanotechnology (AIBN)
The University of Queensland, Brisbane, Australia
E-mail: y.yamauchi@uq.edu.au

Supporting information for this article is given via a link at the end of the document.

mesochannels; ii) larger pores (1.5 – 4 nm): likely form when adjacent micelles come in contact or merge during the condensation of SiO_2. The perovskite precursor solution can access the entirety of the mesoporous film because the main mesoporous channels have less resistance while the interconnecting pores prevent dead-end channels (see **Scheme 1**). When the precursor solution begins to evaporate, it retreats and dewets the surface of the channels. Surprisingly, this solution dewetting effect spontaneously forms 3.1 nm $CsPbBr_3$ perovskite NCs in the interchannel pores. Some larger NCs formed in the mesochannels, but they are a minority product. This approach enables the fabrication of blue-emitting nanocomposites consisting of stable all-inorganic lead halide perovskite NCs in a pre-synthesized mesoporous silica film.

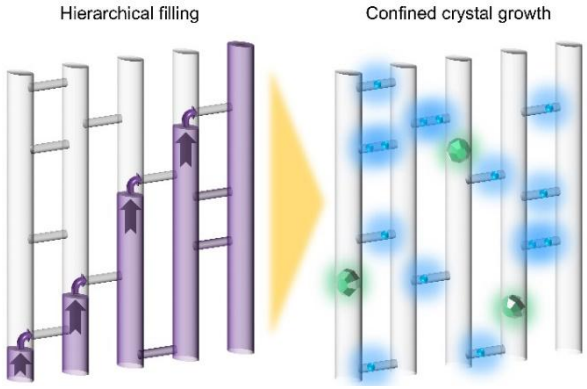

Scheme 1. *Schematic illustration of the hierarchical filling (left image) where the precursor solution infuses the network via the larger channels and smaller interconnecting pores. As the solution evaporates and dewets the channels, small amounts are trapped in the smaller pores, crystallizing to form $CsPbBr_3$ NCs (right image). Although some crystallization occurs in the larger main channels to form green emitting NCs, it mostly takes place in the interconnecting pores, thus the primary emission comes from the small blue-emitting NCs.*

The mesoporous films are prepared by spin-coating glass or silicon substrates with a sol-gel solution of silica precursor (tetraethylorthosilicate) containing a precise concentration of triblock copolymer (EO_{20}-PO_{70}-EO_{20}, Pluronic P123) that yields a 2D hexagonal mesophase of in-plane cylindrical micelles. The polymer and residual solvent was then removed via thermal treatment (see supporting information for detailed procedure). An SEM image of the top surface of the pristine mesoporous silica film (**Figure 1a**) highlights the curved mesochannels domains that are uniformly distributed throughout the sample and appear continuous over several micrometers. After casting and annealing the $CsPbBr_3$ perovskite solution onto the mesoporous substrate, the surface of the sample appears to be filled with nanoparticles, evidenced by the bright contrasting regions inside the channels (**Figure 1b**). The average channel width and the 2D hexagonal mesoporous periodicity remains unaffected, as supported by the SAXS patterns in the inset (pore-to-pore distance of $2 \times d_{\bar{1}2} \approx 10.4$ nm). The semi-elliptical shape of the SAXS pattern is the direct consequence of the distortion induced on the mesoporous structure. It is known that after calcination of the templated film, the periodicity along the vertical axis shrinks and the pores adopt an elliptical shape.[11]

The STEM image in **Figure 2a** shows a typical region of the mesoporous film containing the perovskite nanoparticles. Large crystals arranged along the direction of the channels can be observed, suggesting an effective penetration of the precursor solution during the synthesis. The lateral length of these particles (perpendicular to channel orientation) spans from 5.0 to 8.0 nm. This broad size distribution is caused by the elliptical shape of the mesopores, observed from random orientations under TEM. The complementary high-resolution (HRTEM) images (**Figure 2b-c**) evince the crystallinity of the perovskite particles, with lattice fringes aligned in the direction of the encapsulating silica channels. FFT analysis of the image (**Figure 2d**) indicates the d-spacing is 2.94 Å, which matches the (004) interplanar distance of cubic $CsPbBr_3$ perovskite (*Pbnm*, ICSD card #97852). This observation suggests that the crystals grow in the <001> direction along the channels. The XRD pattern of the composite film reveals several weaker peaks that support this assignment (see **Figure S1**). There is an ongoing debate right now as to whether such perovskite NCs adopt the cubic or orthorhombic structure,[12] and the slight discrepancies in their respective lattice parameters cannot be resolved with the available instrumentation.

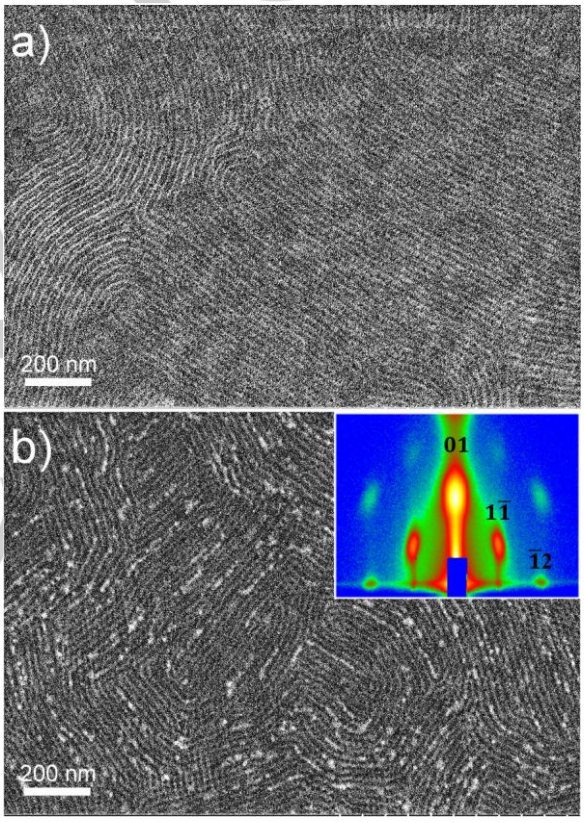

Figure 1. *SEM images of a) the pristine mesoporous silica mesoporous film with channels periodically aligned over > 1 µm, parallel to the surface; b) the $CsPbBr_3$ perovskite-infused mesoporous silica film with several particles (brighter contrast) enclosed inside the channels. Inset: SAXS pattern of the nanocomposite film sample shown in b), attesting that the overall hexagonal periodicity is maintained despite the perovskite inclusion.*

In addition to these NCs, we noticed that the template is riddled with with much smaller particles in the 2.5 to 3.6 nm size range. This bimodal particle size distribution is highlighted by the histogram in the inset of **Figure 2a**. The smaller particles were not observed in the powder sample (see **Figure S2**), although the same precursor concentration was used. This indicates that the smaller particles may originate from how the precursor solution infiltrates and dewets the interior spaces of the template. Furthermore, the adsorption/desorption isotherms revealed that

although the specific surface area of the powder sample is considerably larger, the overall contribution of the interconnecting pores in the film sample is more important (**Figure S3**). As shown in **Figure 1**, the curved mesochannel domains span the surface of the film. Thus infiltration and transport of precursor solution can only pass through the top during the spincoating process. It is possible that the centrifugal force generated by the spin-coating process helps fill the channels. But as mentioned previously, the mesochannels in SBA-15 are interconnected by micropores.[13] A network of large channels and small pores offers innumerable paths for the perovskite precursor solution to permeate the entirety of the film template. When the solution evaporates and retreats, it dewets the surface of the template. The interchannel pores have a lower surface free energy than the solution, so they likely remain filled via a discontinuous dewetting mechanism that is well explained in 2D systems and has been used to grow colloidal nanocrystals.[14] Therefore, the interchannel pores in the films offer two advantages: (i) they offer more paths for the precursor solution to fill the film and (ii) they act as a local discontinuity to trap the solution and direct the growth of perovskites NCs that are small enough to experience quantum confinement and enable blue emission.

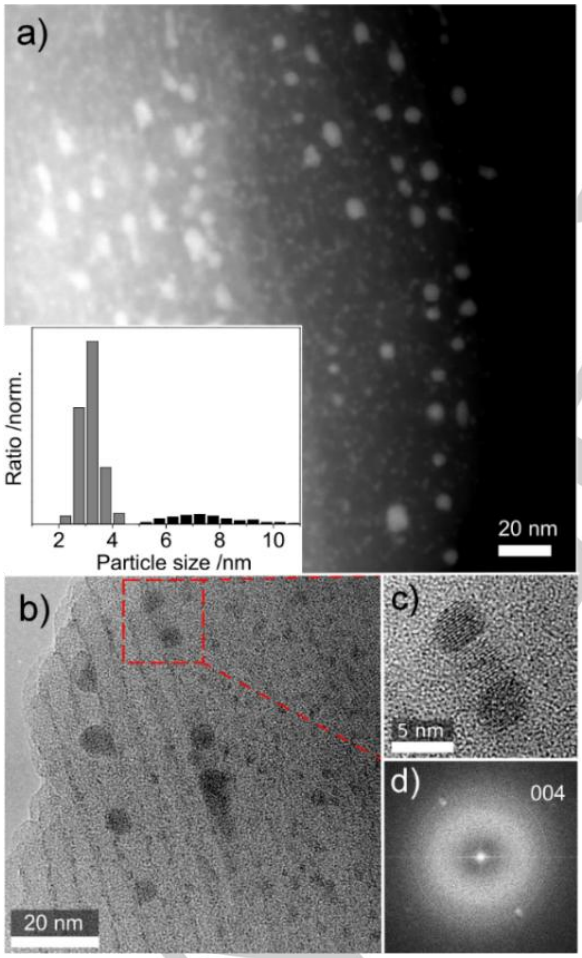

Figure 2. *a) STEM image of the $CsPbBr_3$-infused silica mesoporous film nanocomposite. Inset: histogram highlighting the bimodal particle size distribution, counted over 400 particles. b) Low- and c) high-magnification HRTEM image emphasizing on the $CsPbBr_3$ NCs encapsulated in the mesoporous silica film. d) FFT of the NCs shown in c).*

Figure 3a shows a photograph of $CsPbBr_3$ perovskite NCs in mesoporous powder and mesporous film. The blue emission from the film was further confirmed by the clear displacement of the photoluminescence (PL) peak (**Figure 3b**) compared to the mesoporous powder and bulk perovskite samples. The bulk perovskite has a peak at 525 nm, which is shifted to 507 nm in the mesoporous powder because the quasi-spherical particles experience moderate 3D quantum confinement, expanding the band gap from 2.36 to 2.45 eV. The PL peak from the mesoporous film further shifts to 487 nm, which indicates the particles are much smaller and experience additional confinement (the reproducibility over nine different samples can be assessed in **Figure S4**). Although a band gap of 2.55 eV for crystals ~3.1 nm in size finds supporting evidence in past literature,[8b,15] other publications also reported different values.[2,8d,16] Compared to the bulk, the emission line width of the film sample remain narrow (96 and 108 meV, respectively), suggesting good crystal quality, while the peak for the larger particles in the powder is much broader (144 meV). Due to the location of the emission feature, we can conclude that most of the PL signal emitted from the film sample originates from the smaller crystals formed in the interchannel pores observed by TEM. The peak is asymmetrically shaped, and a double-gaussian fit (white curves) reveals the presence of a weak contribution located at 510 nm, which can likely correspond to the larger 7 nm particles. This is in good agreement with the bimodal distribution discussed earlier. In addition, the resulting excitonic band gap supports the TEM and XRD data that these are likely similar in phase as the larger perovskite NCs. It is also possible that variations in the surface stoichiometry can be partly responsible for this shift, as Br-rich compositions tend to blue-shift the PL features. The overall mechanism describing the formation of nanocrystals in confined spaces is not fully understood, but we assume that the inner walls of the interconnecting pores could impart considerable residual pressure on the surface of the NCs to quench their growth. According to previous study on methylammonium lead halide, it was evidenced that external pressure tends to induce a blue-shift in the PL emission due to amorphization.[17] We decide to rule out this effect, however, since the sharp and intense emission peak does not indicate a disordered structure.

The time-resolved PL curves in **Figure 3c** were fit numerically for each sample with a bi-exponential decay (see **Table S1** in the supporting information). Biexponential fits are frequently used to describe the dynamics of this family of NCs.[12b,18] In our case, the mixed perovskite/air and perovskite/SiO_2 interfaces have dissimilar optical-mode densities and refractive indices and are therefore likely to provide different transition dynamics.[19] The average luminescent lifetime $\langle \tau_L \rangle$ is assessed to be 24.0 ns, thus much shorter than that of the bulk perovskite and mesoporous powders (equal to 41.5 and 53.7 ns, respectively). Confining the growth of $CsPbBr_3$ in a such small volume also led to a substantial increase of the PLQY up to 31.8 % for the films versus 1.6% and 4.1% for the bulk and mesoporos powder sample, respectively. All optical parameters for the three samples are listed in **Table S1**. The fast component of the lifetime τ_1 is slightly larger in the film than in the powder. This result seems counterintuitive at first because the radiative recombination rate typically increases inversely with the crystal size due to larger oscillator strength. The excitonic spontaneous recombination lifetime of surfactant-stabilized $CsPbBr_3$ perovskite NCs, however, has been reported with values ranging between 2 and 8 ns,[12b,18b] suggesting a strong dependence on factors such as the synthetic conditions, morphology and surface passivation.

On the other hand, the mesoporous film has a faster τ_2 (slow component) and larger PLQY than the bulk and powder composite, which results in a strong reduction in the calculated non-radiative lifetime. Presently there is still vigourous debates about the photophysical events that are responsible for the tail of the PL time-response in this family of perovskite materials. If τ_2 can be attributed to trap-assisted mechanisms involving charge capture, thermal release and delayed radiative/non-radiative decays,[20] then our results indicate the nanocrystals generated in the interconnecting pores are well-passivated single crystals that contain minimal defects, hence only a limited amount of surface recombination centers. Others have suggested that photon recycling might lead to longer apparent recombination lifetimes, accompanied by a drastic drop of the external yield compared to the internal quantum efficiency.[21] Here, our results support also this mechanism because the 3 nm crystals in the film are scattered and monodisperse, which reduces the probability for photons to be recaptured.

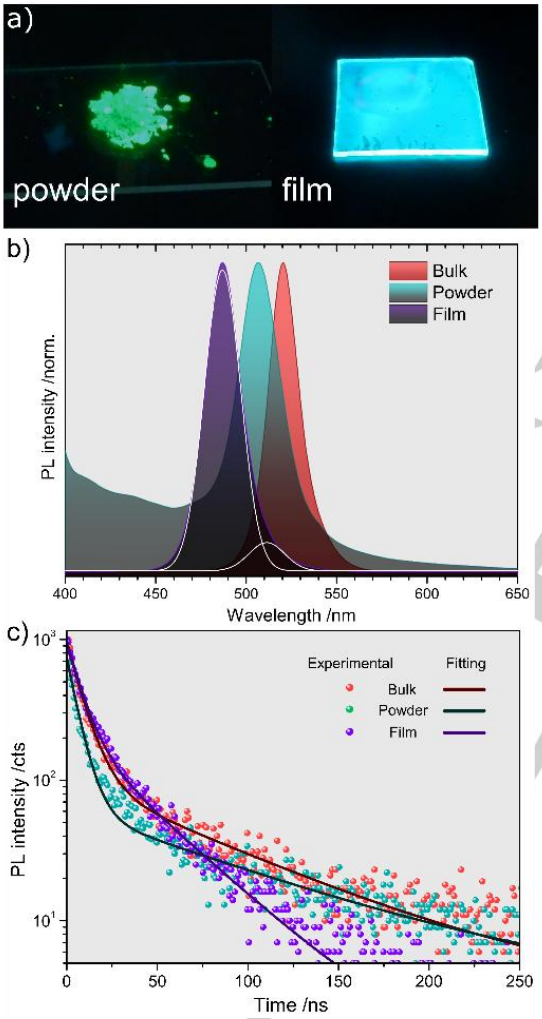

Figure 3. *a) Photograph comparing the powder and film samples under UV light. b) PL spectra comparing the position of the main emission peak for the three samples. The solid white line represents a double-gaussian fitting of the emission peak from the film sample. c) Time-resolved PL decay (λ_{ex} = 365 nm) of the three samples, along with their respective bi-exponential fitting. Fitting parameters are reported in* ***Table S1****.*

The PL emission of the $CsPbBr_3$ mesoporous films should be very stable to various environmental conditions because the NCs are embedded in a composite film. To test stability, one of the film samples was kept under atmospheric conditions (relative humidity 60-70%) in the dark for five months, while another was placed under solar simulated light (λ > 300 nm) for 6 h (see **Figure S5**). In both samples, the PL emission spectra and PL lifetimes and PLQY remained essentially unchanged, showcasing its strong resistance to degradation due to adventitious exposure.

In summary, we demonstrated a simple route to obtain stable blue-emitting $CsPbBr_3$ NCs confined in the interconnecting pores present in adjoining walls of a mesoporous SiO_2 film. These pores are very small and can trap the equivalent of hundreds of yotoliters (10^{-24} liters) of precursor solution that deposits ultra-small blue-emitting $CsPbBr_3$ NCs. We provided sufficient evidence, through electron microscopy and optical measurements, to demonstrate that the blue shift of the film compared to the bulk (ΔE ~ 0.2 eV) is mainly due to strong quantum confinement, although some stress-induced crystallographic distortions are somewhat likely to play a minor role. Compared to the bulk and mesoporous powder sample, the film possesses a shorter PL lifetime and a much higher PLQY. This decrease in non-radiative recombination is combined with a strong resistance to photochemical and moisture-based degradation.

Experimental Section

The starting precursor solution consisted of a stoichiometric mixture of CsBr and $PbBr_2$ dissolved in DMF (0.03 M) stirred at room temperature overnight. From this solution, a bulk reference sample, a powder composite and a film composite were all prepared. The bulk sample was obtained by drop casting the precursor solution on a glass slide. The powder sample was prepared via the previously reported method:[8a] in brief, the perovskite solution was added dropwise to SBA-15 silica powder (synthesized according to [22]) before being vortex mixed vigorously (1 mL/mg). For the composite film, first a sol-gel solution consisting of a mixture of TEOS, P123, H_2O, HCl and ethanol (molar ratio 18.5:1.5:100:0.02:110) was prepared and aged for 3 h, according to a previously published method.[23] The solution was then spin-coated on various substrates (glass, silicon) at 3,000 rpm for 15 s, aged overnight and heat-treated at 400 °C for 5 h, with a ramping of 1 °C/min. The perovskite solution is then spin-casted at 3,000 rpm for 15 s on the mesoporous film. Finally, all three samples (bulk, powder and film) are heat treated on a hotplate at 80 °C, under mild vacuum, for 30 min, followed by 150 °C, in air, for 30 min.

Acknowledgements

This study was supported by an Australian Research Council (ARC) Future Fellow (FT150100479), the Suzuken Memorial Foundation, and JSPS KAKENHI (Grant Numbers 17H05393 and 17K19044). The authors would like to thank Dr. Shirai (NIMS) for helpful suggestion and discussion on materials fabrication.

Keywords: mesoporous silica • mesoporous films • perovskite nanocrystals • confinement • nanospace

[1] Y. Shirasaki, G. J. Supran, M. G. Bawendi, V. Bulović, *Nat. Photonics* **2013**, *7*, 13.

[2] L. Protesescu, S. Yakunin, M. I. Bodnarchuk, F. Krieg, R. Caputo, C. H. Hendon, R. X. Yang, A. Walsh, M. V. Kovalenko, *Nano Lett.* **2015**, *15*, 3692-3696.

[3] X. Li, Y. Wu, S. Zhang, B. Cai, Y. Gu, J. Song, H. Zeng, *Adv. Funct. Mater.* **2016**, *26*, 2435-2445.

[4] H. Huang, F. Zhao, L. Liu, F. Zhang, X.-g. Wu, L. Shi, B. Zou, Q. Pei, H. Zhong, *ACS Appl. Mater. Interfaces* **2015**, *7*, 28128-28133.

[5] S. Gonzalez-Carrero, L. Francés-Soriano, M. González-Béjar, S. Agouram, R. E. Galian, J. Pérez-Prieto, *Small* **2016**, *12*, 5245-5250.

[6] V. K. Ravi, A. Swarnkar, R. Chakraborty, A. Nag, *Nanotechnology* **2016**, *27*, 325708.

[7] Y. Bekenstein, B. A. Koscher, S. W. Eaton, P. Yang, A. P. Alivisatos, *J. Am. Chem. Soc.* **2015**, *137*, 16008-16011.

[8] a) V. Malgras, S. Tominaka, J. W. Ryan, J. Henzie, T. Takei, K. Ohara, Y. Yamauchi, *J. Am. Chem. Soc.* **2016**, *138*, 13874-13881; b) D. N. Dirin, L. Protesescu, D. Trummer, I. V. Kochetygov, S. Yakunin, F. Krumeich, N. P. Stadie, M. V. Kovalenko, *Nano Lett.* **2016**, *16*, 5866-5874; c) V. Malgras, J. Henzie, T. Takei, Y. Yamauchi, *Chem. Commun.* **2017**, *53*, 2359-2362; d) S. Demchyshyn, J. M. Roemer, H. Groiß, H. Heilbrunner, C. Ulbricht, D. Apaydin, A. Böhm, U. Rütt, F. Bertram, G. Hesser, *Sci. Adv.* **2017**, *3*, e1700738; e) M. Anaya, A. Rubino, T. C. Rojas, J. F. Galisteo-López, M. E. Calvo, H. Míguez, *Adv. Opt. Mater.* **2017**, *5*, 1601087.

[9] R. B. Schoch, J. Han, P. Renaud, *Rev. Mod. Phys.* **2008**, *80*, 839.

[10] a) M. Kruk, M. Jaroniec, C. H. Ko, R. Ryoo, *Chem. Mater.* **2000**, *12*, 1961-1968; b) A. Galarneau, H. Cambon, F. Di Renzo, R. Ryoo, M. Choi, F. Fajula, *New J. Chem.* **2003**, *27*, 73-79.

[11] a) Y. Yamauchi, M. Sawada, A. Sugiyama, T. Osaka, Y. Sakka, K. Kuroda, *J. Mater. Chem.* **2006**, *16*, 3693-3700; b) C. W. Wu, Y. Yamauchi, T. Ohsuna, K. Kuroda, *J. Mater. Chem.* **2006**, *16*, 3091-3098.

[12] a) P. Cottingham, R. L. Brutchey, *Chem. Commun.* **2016**, *52*, 5246-5249; b) A. Swarnkar, R. Chulliyil, V. K. Ravi, M. Irfanullah, A. Chowdhury, A. Nag, *Angew. Chem. Int. Ed.* **2015**, *54*, 15424-15428.

[13] H. K. M. Tanaka, Y. Yamauchi, T. Kurihara, Y. Sakka, K. Kuroda, A. P Mills Jr, *Adv. Mater.* **2008**, *20*, 4728-4733.

[14] a) R. J. Jackman, D. C. Duffy, E. Ostuni, N. D. Willmore, G. M. Whitesides, *Anal. Chem.* **1998**, *70*, 2280-2287; b) J. E. Barton, T. W. Odom, *Nano Lett.*; **2004**, *4*, 1525-1528; c) J. Henzie, J. E. Barton, C. L. Stender, T. W. Odom. *Acc. Chem. Res.* **2006**, *39*, 249-257.

[15] J. Butkus, P. Vashishtha, K. Chen, J. K. Gallaher, S. K. Prasad, D. Z. Metin, G. Laufersky, N. Gaston, J. E. Halpert, J. M. Hodgkiss, *Chem. Mater.* **2017**, *29*, 3644-3652.

[16] M. C. Brennan, J. E. Herr, T. S. Nguyen-Beck, J. Zinna, S. Draguta, S. Rouvimov, J. Parkhill, M. Kuno, *J. Am. Chem. Soc.* **2017**, *139*, 12201-12208.

[17] Y. Wang, X. Lü, W. Yang, T. Wen, L. Yang, X. Ren, L. Wang, Z. Lin, Y. Zhao, *J. Am. Chem. Soc.* **2015**, *137*, 11144-11149.

[18] a) B. A. Koscher, J. K. Swabeck, N. D. Bronstein, A. P. Alivisatos, *J. Am. Chem. Soc.* **2017**, *139*, 6566-6569; b) F. Di Stasio, S. Christodoulou, N. Huo, G. Konstantatos, *Chem. Mater.* **2017**, *29*, 7663-7667.

[19] E. Yablonovitch, T. Gmitter, R. Bhat, *Phys. Rev. Lett.* **1988**, *61*, 2546.

[20] a) V. S. Chirvony, S. González-Carrero, I. Suarez, R. E. Galian, M. Sessolo, H. J. Bolink, J. P. Martinez-Pastor, J. Pérez-Prieto, *J. Phys. Chem. C* **2017**, *121*, 13381-13390; b) M. Saba, M. Cadelano, D. Marongiu, F. Chen, V. Sarritzu, N. Sestu, C. Figus, M. Aresti, R. Piras, A. Geddo Lehmann, C. Cannas, A. Musinu, F. Quochi, A. Mura, G. Bongiovanni, *Nat. Comm.*, **2014**, *5*, 5049; c) H. Utzat, K. E. Shulenberger, O. B. Achorn, M. Nasilokski, T. S. Sinclair, M. G. Bawendi, *Nano Lett.*, **2017**, *17*, 6838-6846.

[21] J. M. Richter, M. Abdi-Jalebi, A. Sadhanala, M. Tabachnyk, J. P. H. Rivett, L. M. Pazos-Outón, K. C. Gödel, M. Price, F. Deschler, R. H. Friend, *Nat. Comm.*, **2016**, *7*, 13941.

[22] D. Zhao, J. Feng, Q. Huo, N. Melosh, G. H. Fredrickson, B. F. Chmelka, G. D. Stucky, *Science* **1998**, *279*, 548-552.

[23] Y. Yamauchi, M. Sawada, M. Komatsu, A. Sugiyama, T. Osaka, N. Hirota, Y. Sakka, K. Kuroda, *Chem. - Asian J.* **2007**, *2*, 1505-1512.

Table of Content

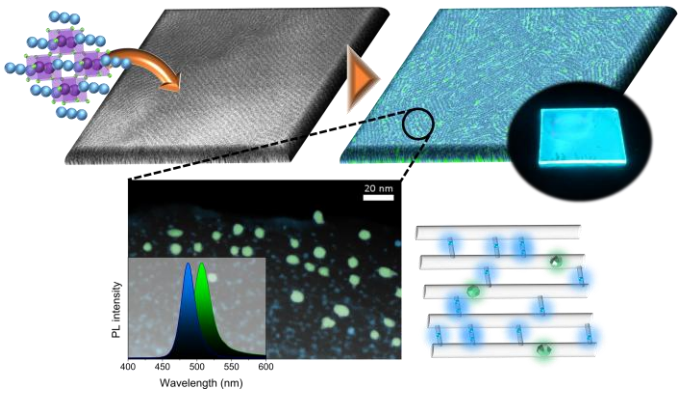

Creating $CsPbBr_3$ perovskite nanocrystals with bright blue emission is challenging because colloidal isolation and purification procedures cause instability. Growing perovskites in mesoporous templates bypasses purification issues because the size of the nanocrystal is governed by the diameter of the pores. Films of aligned mesoporous silica templates can be assembled on surfaces with pore diameters of ~7.5 nm. These mesopores overlap in numerous locations generating tiny, ~1.5 to 3.0-nm diameter interconnecting pores. The hierarchical nature of the porous structure enabled us to easily fill these interconnecting pores with perovskite precursor, and generate stable blue-emitting perovskite nanocrystals (~3.1 nm) that are well-distributed throughout the film. The mesoporous template also serves as a protective barrier to preserve their optical properties from atmospheric conditions. We observe a decrease of the longer lifetime component in the film, accompanied by a drastic increase of the luminescence quantum yield, resulting in a reduction of non-radiative recombination.